A molecular beam study of nonlinearity in the CO-induced surface restructuring of Ir{100}

T. Ali, B. Klötzer, A. V. Walker, and D. A. King

Citation: The Journal of Chemical Physics **109**, 10996 (1998); doi: 10.1063/1.477738
View online: http://dx.doi.org/10.1063/1.477738
View Table of Contents: http://scitation.aip.org/content/aip/journal/jcp/109/24?ver=pdfcov
Published by the AIP Publishing

A molecular beam study of nonlinearity in the CO-induced surface restructuring of Ir{100}

T. Ali, B. Klötzer, A. V. Walker, and D. A. King
Department of Chemistry, University of Cambridge, Lensfield Road, Cambridge CB2 1EW, United Kingdom

(Received 10 August 1998; accepted 18 September 1998)

The kinetics of CO chemisorption on both the (1×5) and (1×1) surfaces of Ir{100}, including the CO-induced surface restructuring process, have been studied by measuring the sticking probability as a function of the surface temperature and beam flux. Due to competition between desorption from the (1×5) phase and growth of (1×1) islands, the sticking probability on the initial (1×5) surface is strongly flux-dependent at surface temperatures T_s in the range $480\leqslant T_s\leqslant510$ K. It is shown that this is due to a strongly nonlinear dependence of the (1×1) growth rate on the local CO coverage on the (1×5) substrate, with an apparent reaction order of around 5. Desorption energies and pre-exponentials of desorption for CO from both the (1×1) and (1×5) surfaces have been determined by means of a modified lifetime measurement technique. Equilibrium coverages as well as isothermal desorption rates of CO were determined for both surface phases. The zero coverage desorption energy of CO from the (1×1) substrate is 196 ± 5 kJ/mol and from the (1×5) surface it is around 150 kJ/mol. This difference in adsorption energies is the driving force for the CO-induced (1×5) to (1×1) phase transition. TEAS data show that the local CO coverage on the growing (1×1) islands during the phase transformation is 0.5 ML. © *1998 American Institute of Physics.* [S0021-9606(98)70348-4]

I. INTRODUCTION

The stable clean Ir{100} surface is reconstructed to a quasihexagonal top Ir atom layer,[1–6] which bears some similarities to the hexagonal structures on the {100} surfaces of Pt and Au. In contrast to Pt{100} the thermodynamically stable structure exhibits a (1×5) LEED pattern due to a fit of the hexagonal layer to the substrate in bridge registry.[2,3] It is lifted to a (1×1) phase by various adsorbates.[4,6–9] Stable and adsorbate-free surfaces of both Ir{100}-(1×1) and Ir{100}-(1×5) can be obtained by controlling experimental conditions.[2–4,6,7] The clean metastable (1×1) phase is kinetically stable up to temperatures as high as 800 K, unlike Pt{100}-(1×1) which reconstructs at around 400 K. The activation energy for the (1×1) to (1×5) phase transition has been determined by two independent studies, both of which revealed a value of about 0.9 eV.[2,4] A recent theoretical study[10] revealed a high activation barrier for self-diffusion of Ir atoms on the Ir{100} surface. A study of NO adsorption on Ir{100} has shown that the reconstruction is not lifted immediately at 300 K, in contrast to the Pt{100} surface.[9] Dosing of CO onto an Ir{100}-(1×5) surface caused only local lifting of the (1×5) reconstruction, as shown by EELS.[7]

No previous molecular beam study has been made of CO adsorption on Ir{100}. Studies of the kinetics and dynamics of the adsorbate-induced restructuring of Pt{100}-hex to (1×1) by CO (Refs. 11, 12) and D_2 (Ref. 13) adsorption revealed a nonlinear growth law for the new phase, i.e., $r_{1\times1}=c(\theta_{\mathrm{hex}})^n$, where $n\approx4$. In a series of papers from this laboratory, it has been demonstrated that this nonlinear term is crucial to the appearance of oscillations in the following catalytic processes on Pt{100}: CO oxidation with NO;[14,15] CO oxidation with O_2;[16,17] and NO reduction with H_2,[18,19] as recently reviewed.[20] Little preliminary knowledge exists about the CO-induced surface phase transition on Ir{100}. Here we extend our earlier work on the kinetics of CO adsorption on Pt{100} to the Ir{100} surface. The method used in the earlier studies[11,12] was modified in order to obtain a dynamic measurement of both the island growth rate and the simultaneous CO coverage on the (1×5)-substrate during the CO-induced lifting of the reconstruction.

II. EXPERIMENT

The clean single-crystal Ir{100} surface (9 mm diam$\times$1.7 mm thick) used in the experiments was oriented within 0.5° of the bulk {100} plane and mechanically polished. Initially, the Ir{100} surface was extensively cleaned by frequent cycles of prolonged Ar ion sputtering at 900 K, annealing at up to 1500 K and oxygen treatment at 1160 K. Routine cleaning involved short occasional Ar ion sputtering at room temperature followed by annealing at 1400 K, oxygen treatment at 1160 K, and finally flashing to 1400 K in vacuum. After this procedure the surface exhibited the reconstructed (1×5) LEED pattern with low background intensity and AES spectroscopy showed impurities to be below the detection limit. After preparing the crystal in this way, a reproducible CO TPD spectrum was obtained and a very intense specular He scattering signal pointed to a well-annealed and clean surface. The clean unreconstructed (1×1) surface was prepared by the method described previously.[2,3] The dual supersonic molecular beam system has been described elsewhere.[12,21] CO gas with a purity of 99.99% vol (Messer–Griesheim) was used in the adsorption experiments.

A. Sticking probability and TEAS measurements

Pure or seeded CO gas was expanded from ~1 atm through the beam nozzle (50 μm in diameter) into the source stage of the molecular beam system, at pressures $10^{-6}-10^{-5}$ mbar. This yields supersonic expansion and isentropic cooling of the gas, which exhibits a very narrow energy distribution. A molecular beam is formed via a cone-shaped skimmer, a collimator and a variable size aperture limiting the beam diameter (at minimum 1.5 mm at the sample surface). Two stage differential pumping provides a pressure of $\sim 1\times 10^{-10}$ mbar in the main chamber. For TEAS experiments during adsorption the CO is mixed with He in a 2 ℓ stainless steel mixing cylinder. Scattering measurements are performed using a high speed rotating chopper (75 Hz) in the second stage of the beam-forming chamber and a rotatable QMS in a differentially pumped housing, which is situated in the scattering plane and capable of angularly resolved line-of-sight detection of desorbing or directionally scattered species. Phase-lock techniques are employed to improve the signal to noise ratio and to reduce the QMS background signal during the scattering experiments. TEAS is used as a dynamic, nondestructive probe of CO distribution and (1×1) island formation during the adsorbate-induced restructuring process. Thus, a simultaneous measurement of the relative specular helium reflectivity and the CO sticking probability is possible. Only the intensity of the specular diffraction signal was monitored, as a function of exposure time; no other (higher order) diffraction intensities could be observed from Ir{100}.

TPD spectra and isothermal pressure curves were recorded by means of a second QMS in the main chamber, which detects a random flux of thermally desorbed molecules. For all TPD experiments a heating rate of 4 K/s was used. The coverage of adsorbed CO is determined from the integral area of the thermal desorption spectra and calibrated to the saturation CO coverage TPD from the (1×1) substrate. A saturated CO $c(2\times 2)$ adlayer with a surface concentration of 6.6×10^{14} molecules/cm^2 (0.5 ML) (Ref. 7) was observed after an exposure of 300 s at 0.1 ML/s on the metastable (1×1) surface. In this paper, surface coverages in monolayers (ML) are quoted relative to the density of Ir atoms in the ideal (1×1) surface of 1.32×10^{15} atoms/cm^2.

Absolute (net) sticking probabilities as a function of exposure time were measured by the King and Wells beam reflectivity method.[22] Small corrections in the time dependent pressure curve were necessary since the pumping speed during the sticking probability experiments changed slowly. The present system is pumped by a 6 in. oil diffusion pump with a liquid nitrogen cooled cold trap plus a titanium sublimation pump (TSP). Before any experiment, the base pressure in the main chamber was less than 1×10^{-10} mbar. Once the beam entered the main chamber, a slight decrease in the effective pumping speed was observed due to slow saturation of the chamber walls with CO. It was important to maintain a very good state of the TSP in order to keep this pressure increase as small as possible. In order to compensate for the residual effect, a reference experiment using exactly the same conditions was performed after every sticking probability experiment. Instead of adsorbing CO onto the sample, the beam was directed onto an inert beam flag mounted in the main chamber. The reference experiment was corrected for the additional pumping effect of the crystal during the sticking probability experiment. The corrected reference curve was obtained by integration of both the sticking probability and the reference experiments up to the same total exposure of the chamber to CO. The reference value at this exposure was used for the final analysis. This procedure is based on the assumption that the effective pumping speed depends only on the total exposure of the chamber walls to CO (thus excluding flux dependent wall effects), and was tested by plotting the reference curves for different beam fluxes vs total exposure. A comparison of the shapes of the resulting curves showed very good agreement, strongly supporting the underlying assumption. By this means it was possible to avoid any assumptions about the change of pumping speed of the system during an experiment.

For any sticking experiment the small final sticking probability on the almost saturated surface was determined by closing the King and Wells (KW) flag and monitoring the resulting small pressure increase and the subsequent trace while the beam is not impinging on the sample. The whole experiment was only considered reliable when a satisfactory fit of the corrected reference experiment to the trace of the sticking probability curve after closing the KW flag was obtained. The sticking probability at time t is then given by

$$s(t)=\frac{p_i-p(t)}{p_i-p(b)}, \tag{1}$$

where p_i is the corrected reference pressure at time t due to the total reflection of the beam off the inert KW flag, $p(t)$ is the pressure due to the reflection of the beam off the crystal, and $p(b)$ is the background pressure of CO. Integration of $s(t)$ yields relative coverages vs time. After calibration to absolute coverages by means of the ratio of the TPD area measured at the end of any sticking probability experiment and the saturation (0.50 ML) TPD area, plots of the net sticking probability vs absolute coverage were obtained. The error in the absolute coverage calibration is estimated to be $\pm 7\%$. A calibration of the beam fluxes was derived from the ratio of absolute adsorption rate and the absolute sticking probability at the very beginning of the CO exposure. The result was compared with already existing flux measurements obtained with a spinning rotor gauge.[23]

B. Heats of adsorption

In order to determine the activation energy for desorption, and hence the heat of adsorption, for CO on the (1×5) and the (1×1) phases, a modified lifetime measurement technique was used. The molecular beam was chopped with low frequencies between 0.05 and 1 Hz by means of a high precision stepper motor operating the KW flag situated in the main chamber. A digital storage oscilloscope was used to average over approximately 100 individual cycles in order to improve the signal to noise ratio. The change of the am-

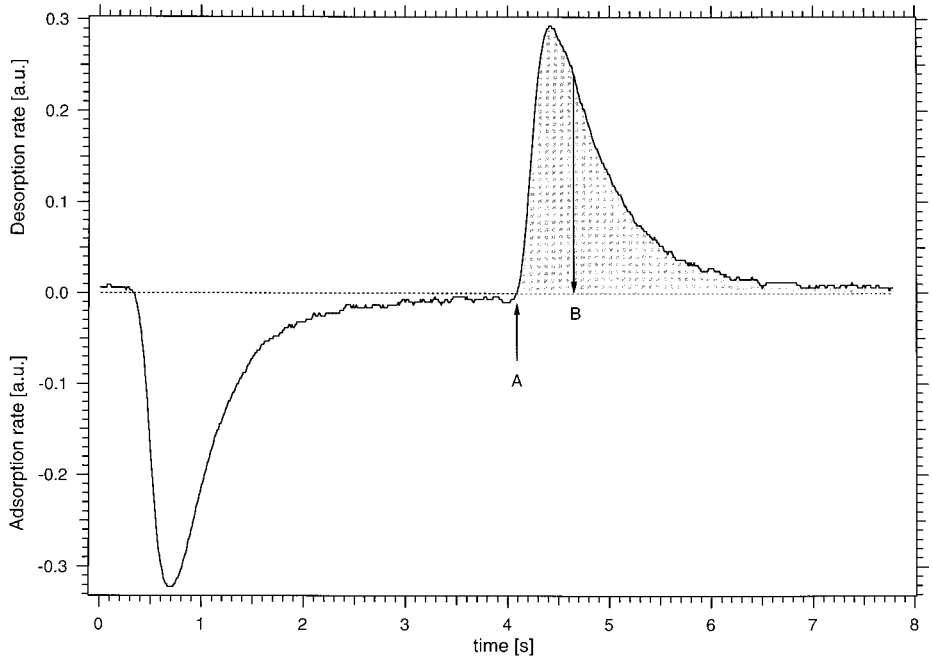

FIG. 1. A typical adsorption–desorption cycle from an initial Ir{100}-(1×1) surface at $T_s=620$ K and a beam flux of 0.052 ML/s. These data are used in the modified lifetime measurement technique described in the text. At A the KW flag is moved between the crystal and the beam source. From B onwards the time constant of the QMS no longer influences the actual trace of the isothermal desorption rate.

bient CO partial pressure in the main chamber was monitored by a QMS detecting a random flux of scattered and desorbing CO molecules. Thus changes in the CO partial pressure were recorded in the same way as for the usual KW sticking probability measurements. The pressure vs time curve exhibited an adsorption trough when the beam hit the crystal and a desorption peak upon interception of the beam by the KW flag (Fig. 1). The pressure changes caused by adsorption and desorption from the crystal were small (less than 5%) compared to the total CO pressure in the main chamber. A short while after allowing the molecular beam into the chamber, an equilibrium situation was established between the background pressure of CO caused by the incoming beam and CO adsorbed on the chamber walls, as discussed above. The process of CO adsorption on the chamber walls, usually in the range of minutes, is much slower than the adsorption process on the crystal and therefore does not affect the pressure vs time behavior of our lifetime experiments. Under the assumption of a constant pumping speed, the pressure change shown in Fig. 1 (after subtraction of the constant offset caused by the equilibrated background CO pressure) is proportional to the net rate of adsorption and desorption from the sample. The total desorbed (and adsorbed) amount of CO can be determined by comparing the small isothermal desorption (and adsorption) peak of the lifetime experiment with a TPD obtained from the $c(2\times2)$ structure. The calibrated peaks can be used to readily derive the absolute rates of desorption (and adsorption).

Two control experiments were carried out to test the validity of our method. Firstly, the crystal was heated to 800 K, where no measurable adsorption effects occur. This experiment resulted in a flat baseline, which clearly excludes the possibility of any adsorption processes other than those occurring on our sample. The same result was obtained by beaming onto on inert glass window situated in the chamber. The second experiment involved comparison of the areas of the adsorption and the desorption peaks, e.g., in Fig. 1. The two areas must be equal, within the experimental error limit. This check was best performed using a very low chopping frequency such that complete adsorption/desorption of CO took place within every cycle, at any given surface temperature. A typical experiment, shown in Fig. 1, indicates that the integrated peak areas above and below the baseline differ by less than 2%. The most important aspect of these measurements is that they can be used to determine the equilibrium adsorbed amount of CO for a given beam flux and a given sample temperature. A variation of the sample temperature at a constant beam flux yields an adsorption isobar of CO on Ir{100}. Due to the stability of the clean (1×1) phase even at elevated temperatures, adsorption isobars could be measured separately on both the (1×5) and the (1×1) substrate. The (1×1) substrate is not converted back to the (1×5) at temperatures where desorption of CO is sufficient for the lifetime experiments (700 K was the maximum sample temperature used for these measurements—the clean (1×1) is stable up to 800 K). The coverage on the (1×5) was always kept very small so that transformation towards the (1×1) surface was negligible during the measurements. In addition, the experiments were performed at temperatures exceeding 580 K, well above the temperature where flux dependent CO adsorption was observed. Values for the activation energies for desorption from both (1×1) and (1×5) phases were determined from an isosteric analysis of the isobars. As a reasonable approximation it was assumed that the heat of desorption equals the activation energy for desorption of CO. This value was then used to determine the desorption pre-exponential from the isothermal desorption peaks. The kinetic analysis of the desorption rate vs coverage was performed in the coverage range where the rates are no longer influenced by the chosen time constant of the QMS.

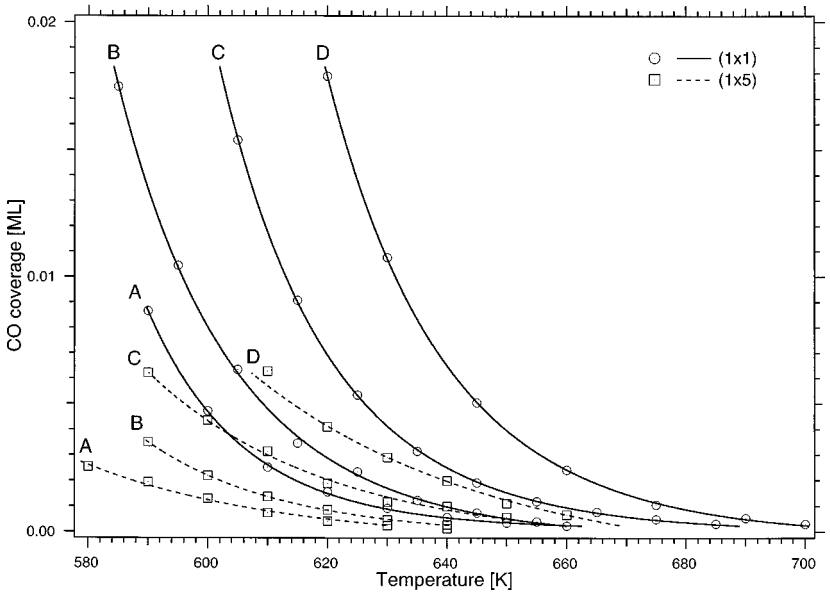

FIG. 2. Measured isobars of CO on the metastable Ir{100}-(1×1) (solid lines) and the stable Ir{100}-(1×5) surface (dashed lines). The beam fluxes were 0.0083 (A), 0.015 (B), 0.052 (C) and 0.124 ML/s (D) in both cases.

III. RESULTS AND DISCUSSION

A. Isosteric heats and lifetime measurements

In order to obtain heats of adsorption of CO on the (1×1) and the (1×5) phases of Ir{100}, in the latter case *without* lifting the reconstruction, isosteric and lifetime measurements were made on each surface. Measured isobars of CO on Ir{100}−(1×5) and (1×1) are shown in Fig. 2. Each data point represents the average of at least 64 individual measurements. The equilibrium coverage on the (1×5) substrate is about 4 times lower than on the (1×1) at the same flux and sample temperature, T_s. Thus the relative error in the determination of the heat of adsorption from an isosteric analysis was considerably smaller in the case of the (1×1) substrate. Of course, lowering T_s and increasing the flux would generate similarly high CO coverages on the (1×5) substrate, but these were intentionally kept low in order to avoid any (1×1) island formation. A least squares fit of the function

$$\theta = a e^{b/T} \tag{2}$$

was tested for the (1×1) isobars, since the integration of Van't Hoff's equation yields a function of this form. For all four isobars from the (1×1) substrate a very good fit was obtained (Fig. 2). The uncertainty in the experimental coverages is between 2% and 6% which arises from the noise in the pressure readings and the uncertainty in the baseline correction (see Fig. 1). The resulting fits were always well within the experimental error limit. The fitted curves were then used to extract isosteres from the present data and to determine the heat of adsorption as a function of CO cover-

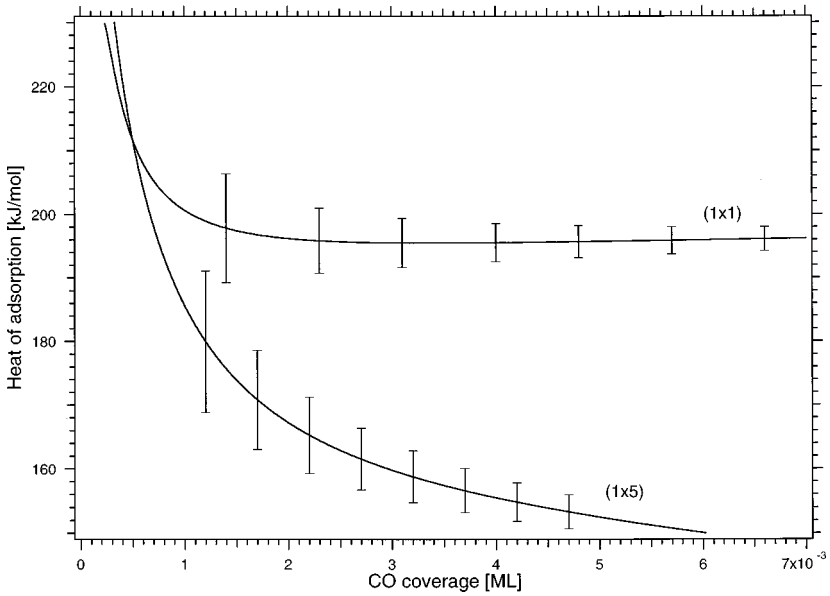

FIG. 3. Isoteric heats of adsorption as a function of CO coverage on the (1×1) and the (1×5) surfaces of Ir{100} in the coverage range 0–0.007 ML, derived from an analysis of the adsorption isobars in Fig. 2.

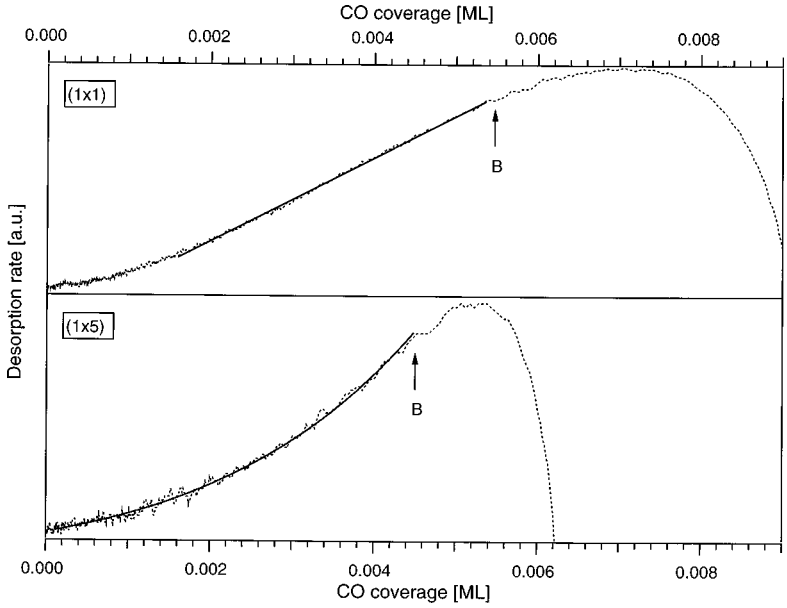

FIG. 4. Isothermal desorption rates of CO at $T_s = 600$ K from Ir{100}-(1×1) (top figure) and Ir{100}-(1×5) (bottom figure) as a function of the respective CO coverages. Dashed lines, experimental data; solid lines, calculated rates on the basis of first order desorption. In the top graph for the (1×1) surface a constant desorption energy of $E_d = 196$ kJ/mol was used, obtained from Fig. 3, yielding a first order desorption pre-exponential of 3.1×10^{14} s^{-1}. The bottom figure is based on a linear coverage dependence of the desorption energy, $E_d = (150-100\theta)$ kJ/mol, from which a first order desorption pre-exponential of 6×10^{13} s^{-1} was derived. Point B corresponds to the same point marked in Fig. 1.

age (Fig. 3). Above a total coverage of 0.002 ML, the isosteric heat of adsorption on the (1×1) surface was found to be coverage independent, within experimental error, and a value of 196±5 kJ/mol was derived from the plateaulike section in Fig. 3. Below this coverage, a strong increase of the adsorption heat is observed, which is attributed to adsorption on defect sites.

The average isosteric heat of adsorption on the (1×1) surface was taken as the basis for further analysis. Rate constants for isothermal desorption traces were determined from 15 independent isothermal desorption traces from the (1×1) substrate (as shown in the top graph in Fig. 4). Using the mean value of 196 kJ/mol for the (1×1) desorption energy, a set of first order pre-exponentials were determined, yielding a mean value of $3.1\pm1.6\times10^{14}$ s^{-1}. Strong support for a constant, coverage-independent desorption energy comes from the first order analysis of the isothermal desorption rates from the (1×1) substrate. Plots of the desorption rate vs coverage exhibit a significant linear region for all (1×1) experiments (top graph, Fig. 4). Nonlinearity in the (1×1) plot for coverages below 10^{-3} ML is directly attributable to the rise in adsorption heat below this coverage (Fig. 3), which we assign to adsorption on defects.

The isosteric analysis of the (1×5) isobars was again achieved by interpolation of the data points in the same way as for the (1×1), but due to the larger relative error in the data, a poorer fit was obtained (dashed traces in Fig. 2). The plot of the isosteric heat of adsorption of CO on the (1×5) substrate vs coverage in Fig. 3 shows a pronounced coverage dependency in the range 0.002–0.006 ML. This is in contrast to an almost constant value obtained for the heat of adsorption of CO on the (1×1) phase in the same coverage range. Strong additional support for a coverage dependence on the (1×5) substrate comes from the analysis of the isothermal desorption rates. Again, in contrast to the (1×1) substrate, plots of the desorption rate vs coverage for the (1×5) phase always showed a deviation from strictly linear behavior (Fig. 4, lower graph). Nevertheless, an approximate value for the first order desorption pre-exponential from the (1×5) of 6×10^{13} s^{-1} was derived on the basis of first order desorption kinetics and a desorption energy of 150 kJ/mol, implementing a linear dependence of the desorption energy of around 100 kJ mol^{-1} ML^{-1} from the CO coverage. On this basis a good fit of the calculated to the experimental desorption rates was obtained (Fig. 4).

The fact that the heat of adsorption on the (1×5) surface does not reach a constant final value but continues to drop even at 0.006 ML, can be attributed both to a higher defect concentration on the (1×5) substrate—which are not saturated at coverages above 0.006 ML—and a coverage dependence of the adsorption heat on the well-ordered (1×5) patches. A high defect concentration on the (1×5) surface is likely because of the relatively low annealing temperature of 1400 K. It has been shown[2,3] that $T_s \geqslant 1300$ K is necessary to remove the last traces of (1×1) area and complete the restructuring to the (1×5) surface. On the other hand even 650 K is sufficient to establish a well-ordered (1×1) surface by oxygen adsorption,[4] and the annealing temperature of 740 K in the (1×1) preparation procedure is therefore effective in eliminating defects. Our general impression is that under the present experimental conditions it is easier to establish a well-ordered (1×1) surface than a well-ordered (1×5) surface.

From the experiments discussed in this paper, it is not possible to elucidate whether the CO adsorption energy on the (1×5) surface is influenced by a higher degree of defects or if there is a ''true'' coverage dependence resulting from repulsive interactions between adsorbed CO molecules. However, it is highly unlikely that a repulsive interaction between adsorbed molecules could manifest itself at coverages as low as 5×10^{-4} ML, and we therefore attribute the sharp fall in heat displayed in Fig. 3 to the presence of defects. The minimum sample temperature for the lifetime measurements on the (1×5) was 580 K, yielding a maximum CO coverage of around 0.01 ML (Fig. 2), but the flux-dependent sticking probability experiments (to be discussed

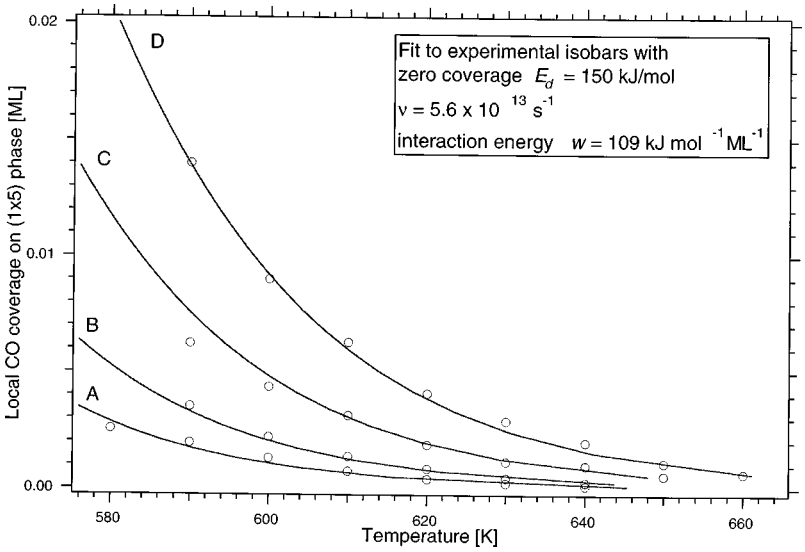

FIG. 5. Solid lines show best fits to the experimental isobars of CO on Ir{100}-(1×5) using a simple Langmuir-type model which includes a linear coverage-dependence of the desorption energy. The labels A–D correspond to the fluxes in Fig. 2.

in the next section) were carried out at 490 K. At this temperature the local CO coverage on the (1×5) substrate is considerably higher. The range of local (1×5)-coverages over which the surface phase transition takes place is around 0.1 ML, as will be shown in the following section. Therefore the experiments will be discussed on the basis of two limiting cases. If the heat of adsorption on the well ordered (1×5) areas was constant at coverages around 0.1 ML where all defects are saturated with CO, the extrapolation of the heat of adsorption on the (1×5) surface in Fig. 3 would approach a constant value well below 150 kJ/mol. In addition it is possible that adsorption on the well-ordered (1×5) patches is determined by a coverage-dependent binding energy. The actual trace for the isosteric heat of adsorption on the (1×5) surface at around 0.1 ML is unknown, but extrapolating the coverage dependence below 0.01–0.1 ML suggests an upper limit of 150 kJ/mol for the heat of adsorption on a defect-free (1×5) surface. On this basis, we attempted to derive a numerical value for an interaction energy as follows. A simple Langmuir model was used to describe the experimental (1×5) isobars of Fig. 2. The lowest measured value for the (1×5) heat of adsorption of around 150 kJ/mol (in Fig. 3) was assumed to be the most realistic value for the zero coverage desorption energy from a defect-free surface. A first order desorption pre-exponential of $6\times10^{13}\ s^{-1}$ was taken from the analysis of the isothermal desorption rates (Fig. 4, lower graph). These values for E_d and ν_d, respectively, were used to obtain a least squares fit to the experimental data points. A reasonable fit could be obtained only by implementing a linear coverage-dependence of the desorption energy. The best fit was obtained with an interaction energy of $109\ kJ\ mol^{-1}\ ML^{-1}$. The calculated isobars and the experimental data points for the (1×5) substrate are shown in Fig. 5.

The results of this section are best summarized in Fig. 6. The adsorption of CO on the unreconstructed (1×1) substrate is energetically more favourable than on the reconstructed (1×5) surface. According to the measured heats of adsorption, 17 kJ/mol (with respect to Ir surface atoms) is gained when chemisorbed CO is trapped from (1×5) areas into the growing (1×1) domains. This energy gain is the driving force for the CO-induced lifting of the reconstruction. In order to derive this value, the energy difference between the clean (1×1) and (1×5) surfaces of Ir{100} is needed. The value of 6 kJ(mol Ir_s)$^{-1}$ used in Fig. 6 is based on a DFT-GGA calculation by Ge and King.[24] We note that an experimental value for the energy difference between the hex and the (1×1) clean surfaces of Pt{100} has been obtained by single crystal adsorption calorimetry, as 12 ± 2 kJ(mol Pt_s)$^{-1}$.[25,26]

B. Sticking probabilities

Figure 7 shows the sticking probability of CO on the

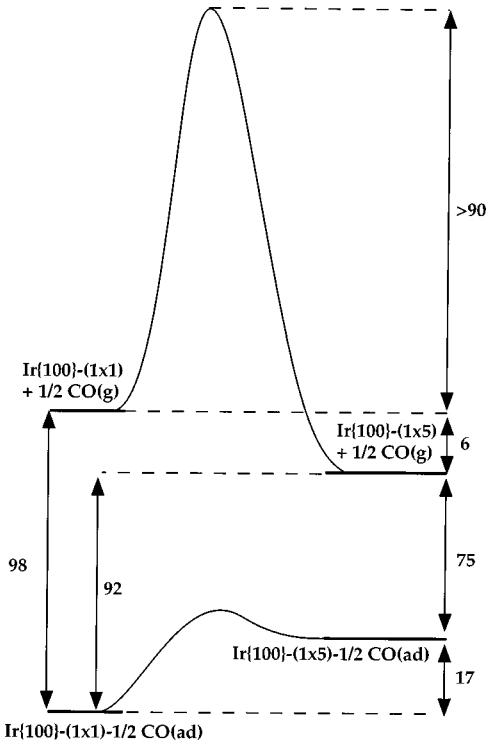

FIG. 6. Schematic energy diagram for the adsorption of CO on Ir{100}. The energies are in kJ/mol of surface iridium atoms.

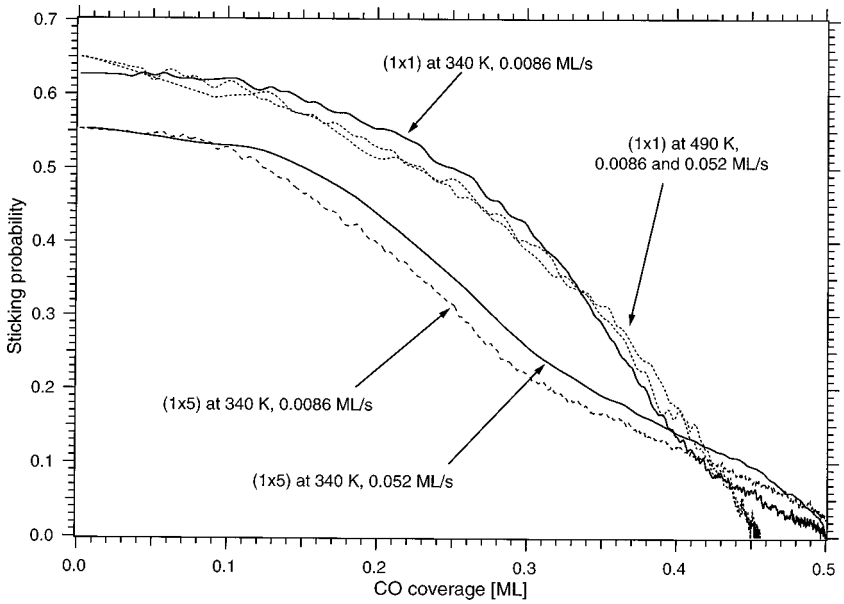

FIG. 7. The sticking probability of CO on the (1×5) and (1×1) phases of Ir{100} at the surface temperatures and beam fluxes indicated. The nozzle was at room temperature in all cases, corresponding to a beam energy of 51 meV.

metastable Ir{100}-(1×1) surface as a function of total CO coverage, θ. Two of the experiments were performed at $T_s = 490$ K at different fluxes, 0.0086 ML/s and 0.052 ML/s, the same conditions which resulted in a pronounced flux dependent sticking probability in the case of the (1×5) surface (cf. Fig. 9). The experiments shown in Fig. 7 clearly exclude a possible flux dependency in the uptake of CO on the (1×1) substrate. Figure 7 also shows sticking probability curves measured on the (1×5) surface at the lower T_s of 340 K, again with fluxes of 0.0086 and 0.052 ML/s. There is no flux dependence in the uptake of CO on the (1×5) substrate if the sample temperature is low enough to avoid any desorption of CO during the sticking probability experiment. The initial sticking probability on the (1×5) surface is 0.55, whereas it is 0.65 on the clean metastable (1×1) substrate.

A comparison of the experiments at 490 and 340 K shows the effect of partial desorption from the complete (1×1) substrate. In this case no change of the shape of the sticking probability curve is observed, but the final coverage is lower in the 490 K experiment. This behavior is to be expected if the net sticking probability is lowered at the end of the experiment, due to partial desorption. In contrast, the shape of the (1×5) experiments at 490 K is strongly influenced by the beam flux (cf. Fig. 9), attributed to nonlinear effects in the phase change dynamics.

The initial sections of the 340 K experiments both on the (1×5) and (1×1) surfaces show a constant sticking probability up to a coverage of 0.1 ML. We conclude that precursor-mediated adsorption is operative on both substrates at ambient temperatures.

Figure 8 displays the sticking probability of CO on an initial Ir{100}-(1×5) clean surface as a function of total CO coverage for different sample temperatures. The initial sticking probability of 0.55 ± 0.03 is independent of T_s. It drops to practically zero above 0.5 ML total CO coverage, which, by analogy with CO adsorption on Pt{100},[11,12] may be taken as the point where the (1×1) islands with 0.5 ML local CO coverage have grown to cover the entire surface. In the case of Ir{100} no preliminary evidence for this assumption could be found in the literature, but TEAS results, which will be discussed later, strongly support it.

LEED observations concomitant with the sticking probability measurements showed that the CO-induced lifting of the (1×5) reconstruction at these temperatures does not result in the formation of a perfect (1×1) substrate. A poorly ordered (1×1), with some residual streaky intensities in the (0,1) and (1,0) directions and a high background intensity, pointed to an incomplete lifting of the reconstruction. After some time, broad and not very intense $(\frac{1}{2}, \frac{1}{2})$ spots appeared. These observations are in accordance with previous LEED studies.[7] The interpretation with ''local'' lifting of the reconstruction implies the formation of many small but out-of-phase $c(2\times2)$-CO domains on the Ir{100}-(1×1) surface. The observed $c(2\times2)$ intensities indicate that the local coverage is 0.5 ML of CO. The formation of a well-annealed (1×1) substrate requires temperatures of at least 740 K. Thus the highest possible adsorption temperature of 500 K (Fig. 6) is not sufficient to produce a well ordered (1×1). Still, most of the surface consists of (1×1)-patches.

Adsorption at 340 K on the clean (1×1) surface up to 0.15 ML reveals an almost constant sticking probability in this coverage range, as shown in Fig. 8, which suggests the influence of precursor-mediated adsorption. This becomes less pronounced as the sample temperature is increased, with the experiment at the highest T_s (480 K) exhibiting an almost perfectly linear decrease with increasing θ_{CO}, in good agreement with large islands of (1×1) growing with a constant local coverage of 0.5 ML, and negligible contribution to island growth from precursor diffusion to island boundaries at this temperature. A further increase of the temperature beyond 480 K induces additional changes in the shape of the sticking probability curves (Fig. 9). The 480 K experiment is just at the borderline where the onset of desorption from the (1×5) substrate can come into play. An increase in T_s of just 5° to 485 K results in a weak break in the sticking probability curve, which causes a slight lowering of the net

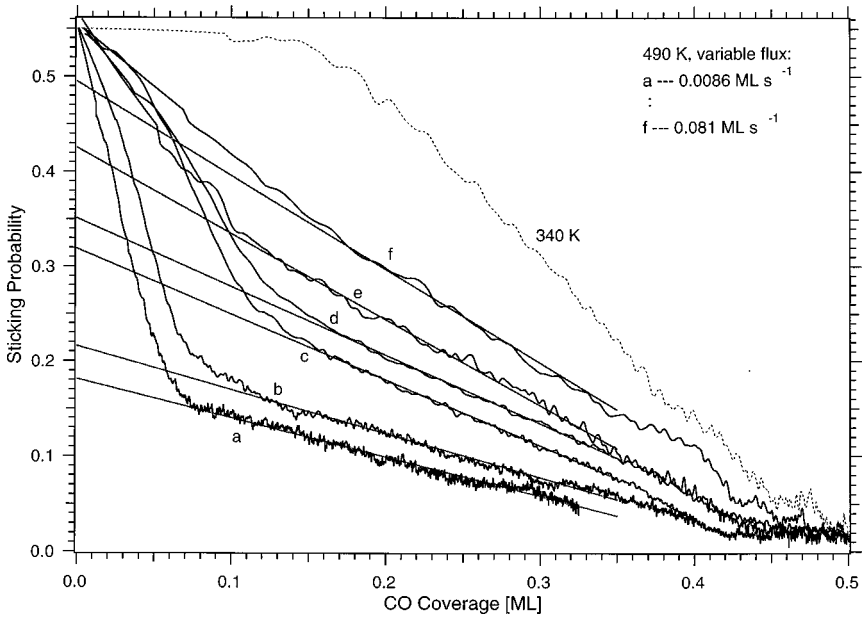

FIG. 8. The measured (net) sticking probability of CO on an initial Ir{100}-(1×5) clean surface as a function of total CO coverage at different normal incidence molecular beam fluxes, as indicated. Nozzle temperature, 300 K. The sticking probability at a sample temperature of 340 K is shown for comparison (flux=0.0052 ML/s).

sticking probability at coverages beyond the break position. Further increases in temperature lead to more pronounced breaks in the sticking probability curves. A TEAS experiment carried out during adsorption at 490 K (shown in Fig. 10, which will be discussed more thoroughly in a later section) also shows a break which clearly demonstrates that a structural change is taking place. The breaks in the 490 K sticking probability and TEAS curves both occur at the same coverage. The TEAS data indicate that the break can be attributed to the onset of the CO-induced lifting of the (1×5) reconstruction.

Depending on the temperature, the breaks in the sticking probability curves tend to occur at different positions on the total CO coverage axis. A significant trend to higher coverages with decreasing T_s can be observed in Fig. 8. The breaks can be seen to become sharper and more pronounced as the sample temperature is increased, which in turn causes an increase in the rate of desorption from the reconstructed (1×5) substrate during the prevailing phase transition. The shift of the break positions to higher coverages with decreasing temperature thus indicates a trend to higher local coverages on the (1×5) and provides at least a qualitative interpretation of the increasing net adsorption rate, and thus island growth rate via the increase of the local coverage on the (1×5). As discussed for CO on Pt{100},[11,12] the island growth rate can be derived from the value of the net sticking probability during the phase change.

Previous studies of the kinetics of the adsorbate-induced restructuring of Pt{100}-hex to (1×1) by CO and D_2 (Refs. 11–13) revealed a nonlinear growth law for the new phase. This growth law can be represented as $r_{1\times1}=c(\theta_{\mathrm{hex}})^n$, where $n\approx4$. The similarity between the results presented in Fig. 8 and those obtained for CO adsorption on Pt{100} demonstrate the same basic underlying mechanism in these two

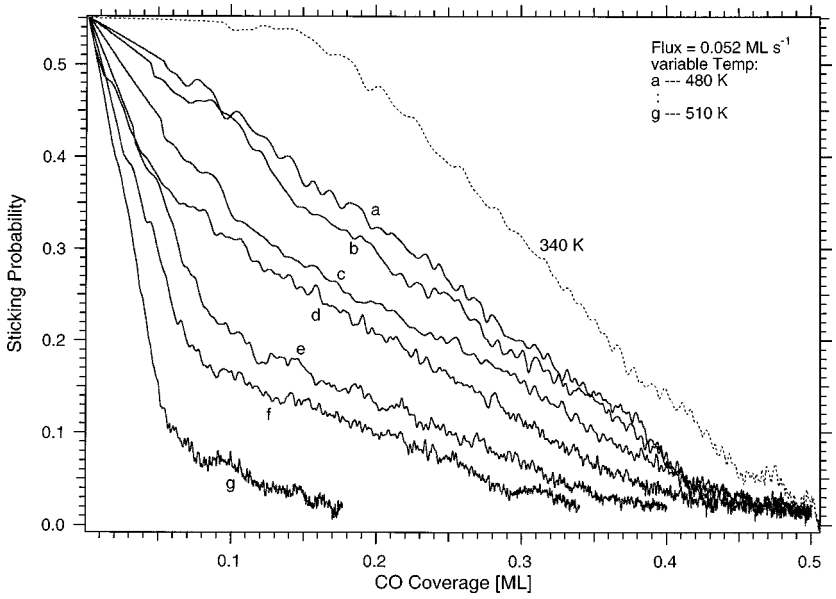

FIG. 9. The net sticking probability of CO on an initially clean Ir{100}-(1×5) surface as a function of total CO coverage. Beam flux=0.052 ML/s and nozzle temperature=300 K. The surface temperature was varied, as indicated, between 490 and 510 K in steps of 5 K.

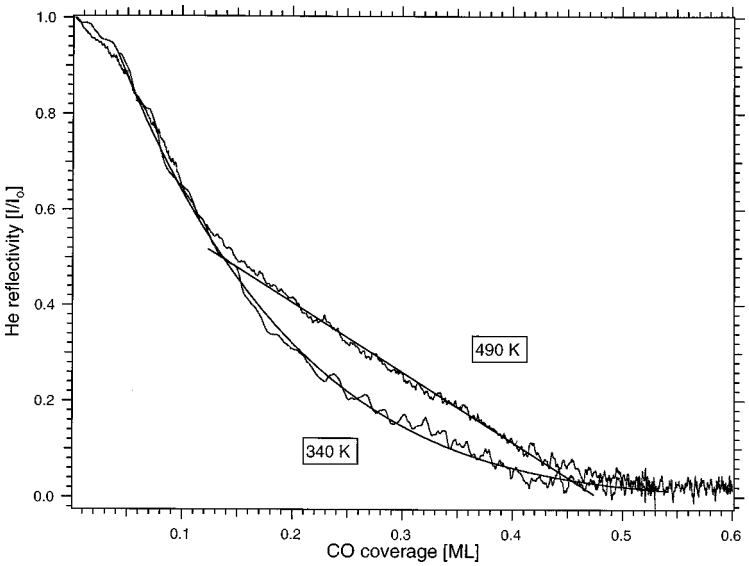

FIG. 10. The specular He reflectivity as a function of total CO coverage on an initial Ir{100}-(1×5) clean surface at 340 and 490 K. The solid curve represents a least squares fit of a simple model for random adsorption, described in the text. The straight line is a guide to the change in slope of the 490 K experiment.

systems. The only major difference is the much higher local CO coverage in the case of the Ir substrate during the phase transformation. This higher CO coverage may not be surprising considering the large barrier to self-diffusion of Ir atoms on the {100} surface.[10] The nonlinear growth law[11–13] contains a pre-exponential which may be interpreted in terms of a probability factor that a local fluctuation of four chemisorbed CO molecules towards the (1×5)-(1×1) phase boundary successfully leads to the formation of an additional (1×1) area. According to the microscopic growth mechanism schematically represented in Fig. 11, local-density fluctuations in the adlayer lead to 4 CO molecules on adjacent substrate atoms, which induce the spatial displacement of about 7–8 Ir atoms at the phase boundary. The probability that this will be converted to (1×1) before the local structure is broken up will depend on the metal–metal bond strength. Hence a much higher local CO coverage on the (1×5) might be required in order to increase the probability for ''successful'' fluctuations. Nevertheless, the power law could still apply. On this basis, a kinetic model of the phase change involves the following steps:

$$n[\mathrm{CO}\text{–}\mathrm{Ir}_{1\times5}] \underset{k_{-1}}{\overset{k_1}{\rightleftharpoons}} (\mathrm{CO})_n\text{–}\mathrm{Ir}_{2n}^{1\times5}, \tag{3}$$

$$(\mathrm{CO})_n - \mathrm{Ir}_{2n}^{1\times5} \overset{k_2}{\rightarrow} (\mathrm{CO})_n - \mathrm{Ir}_{2n}^{1\times1}. \tag{4}$$

We denote the fractional coverage of the surface by $(\mathrm{CO})_n\text{–}\mathrm{Ir}_{2n}^{1\times5}$ ensembles as $\theta_{::}$, and n is the number of local CO molecules required to induce the $(1\times5)\rightarrow(1\times1)$ switch ($n=4$ for CO on Pt{100}), at a local coverage of 0.5 ML. The fractional coverage of single Ir atoms covered by one CO is denoted as $\theta_{\cdot\cdot}$. Then, at steady state,

$$d\theta_{::}/dt = 0 = k_1\theta_{\cdot\cdot}^{n} - k_{-1}\theta_{::} - k_2\theta_{::}. \tag{5}$$

Consequently,

$$k_1\theta_{\cdot\cdot}^{n} = (k_{-1}+k_2)\,\theta_{::}, \tag{6}$$

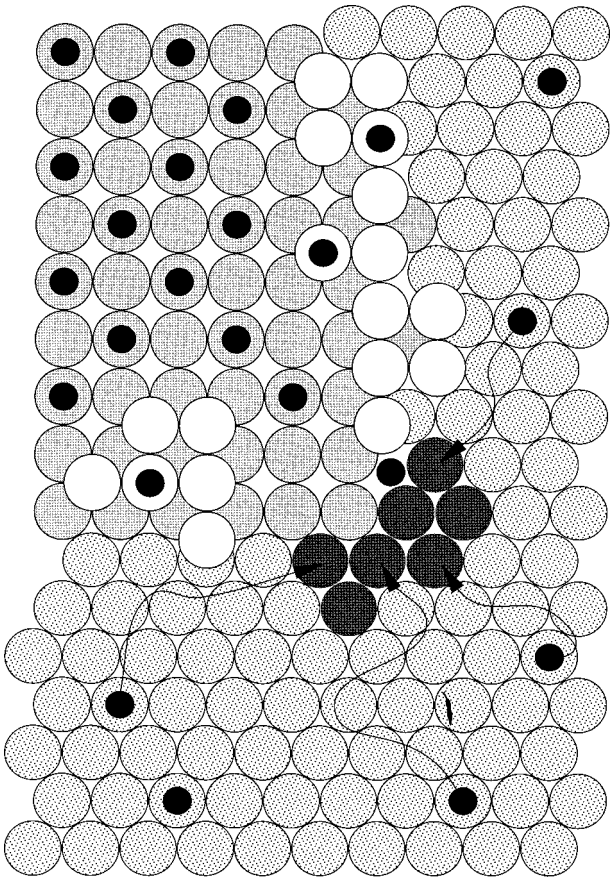

FIG. 11. A schematic illustration of the CO induced $(1\times5)\rightarrow(1\times1)$ phase transformation on Ir{100}. Dotted circles, surface Ir atoms in the (1×5) phase; grey circles, Ir atoms in a growing (1×1) island; small black circles, chemisorbed CO; white circles, excess Ir atoms forced up as a result of the completed phase transformation; dark grey circles, next 7 Ir atoms to be converted to (1×1), induced by a statistical fluctuation of the local coverage on the (1×5) phase in which 4 CO molecules come together (as indicated by the arrows) at the boundary of the growing (1×1) domain.

$$\theta_{::} = \frac{k_1}{k_{-1}+k_2}\,\theta_{\bullet}^{n}. \tag{7}$$

Then the rate of (1×1) growth is

$$r_{1\times1} = k_2\theta_{::} = \frac{k_1 k_2}{k_{-1}+k_2}\,\theta^{n}. \tag{8}$$

This means that the coverage in arrays of n CO molecules on $2n$ adjacent Ir atoms, producing a local coverage of 0.5 ML, depends on the nth power of the CO coverage on the (1×5) substrate. One can now distinguish two limiting cases. In the first, $k_2 \ll k_{-1}$, the situation for a fast equilibrium in advance of a slow irreversible reaction step to (1×1). In the second, $k_2 \gg k_{-1}$, consistent with steady state kinetics with respect to the formation of local arrays of n COs on the (1×5); here the coverage in these arrays remains very small, because they are efficiently converted to CO-covered (1×1)-patches.

In terms of the power law concept[11–13] this means that—in contrast to Pt{100}—the lower mobility of Ir atoms could be responsible for a relatively low value of k_2. Since the flux-dependent sticking probability experiments on iridium were performed at 490 K, about 100 K above the temperature where the platinum experiments were performed,[11,12] values of k_1 and k_{-1} describe the diffusion of CO across the (1×5) surface and are comparable to those on platinum. Since the heats of adsorption of CO on Pt{100}-hex (106 kJ/mol) and $Ir\{100\}$-(1×5) (150 kJ/mol) are not very different, similar activation barriers for diffusion might be expected.

We have determined the reaction order n in the power law expression from our measurements. This was obtained from a series of sticking probability experiments performed at different beam fluxes, while maintaining a constant sample temperature of 490 K. The main advantage of using a constant T_s is that a possible temperature dependence of the power law pre-exponential, $c = k_1 k_2/(k_{-1}+k_2)$, does not come into play and the local CO coverage on the (1×5) surface is only changed via the beam flux. The set of experiments used to determine a value for n are shown in Fig. 9. For comparison, the sticking probability curve at $T_s = 340$ K with a flux of 0.052 ML/s is also shown. The experiment at 0.052 ML/s beam flux compares directly with the experiment at 490 K in Fig. 8 (curve e). Using a higher beam flux (0.081 ML/s, curve f) induces higher island growth rate and the break marking the onset of the CO-induced $(1\times5)\rightarrow(1\times1)$ restructuring almost disappears. Lowering the beam flux causes the breaks to become more pronounced, since the local CO coverage on the (1×5) and thus the rate of (1×1) island growth is lowered. The trend of the break positions again reflects the change of the local CO coverages on the (1×5) substrate. The break position at a given flux for these sticking probability curves are shown in Table I. Within experimental error, the values of the break positions reflect the local CO coverages on the (1×5) during the adsorbate induced restructuring.

Our analyses of the sticking probability experiments is based on two different assumptions; a coverage-dependent, and coverage-independent, desorption energy. We note that the actual shape of the curve for the isosteric heat of adsorption on the (1×5) surface, shown in Fig. 3, is unknown in the coverage range around 0.1 ML.

TABLE I. (1×1) island growth rates and local CO coverages on (1×5) areas during the surface phase transition at 490 K with and without implementation of a coverage-dependent desorption energy.

Beam flux (ML/s)	CO coverage at break (ML)	$\theta_{CO}^{1\times5}$ $E_d=$ 116 kJ/mol	$\theta_{CO}^{1\times5}$ $E_d=$ $150-\theta$ kJ/mol	Island growth rate (ML/s)
0.0086	0.06	0.073	0.083	0.00156
0.0120	0.08	0.092	0.091	0.00259
0.0200	0.12	0.104	0.104	0.00638
0.0290	0.13	0.129	0.114	0.01020
0.0520	0.14	0.140	0.131	0.02210

1. Coverage-independent desorption energy

In the coverage-independent case, a very similar procedure can be applied for the determination of the island growth and local CO coverage on the (1×5) surface to that used for Pt{100}.[11,12] In short, this procedure was based on the assumption that desorption only occurs from the (1×5) substrate, where CO is more weakly bound, and that the contribution of CO desorption from the (1×1) substrate is negligible. In this case the desorption rate r_d from the (1×5) substrate can be derived for any total CO coverage from the difference of the sticking probabilities with and without desorption, i.e., from the *net* and the *absolute* sticking probabilities s_a and s_n, respectively,

$$r_d = Q(s_a - s_n), \tag{9}$$

where Q is the flux. One method is to derive the value for the absolute adsorption rate, Qs_a, from an extrapolation of the experimental net sticking probabilities in Fig. 9 at a given total CO coverage towards infinite flux, following Guo and King;[27] this is achieved by plotting s_n vs $1/Q$. A second method is directly demonstrated in Fig. 9, and includes a least squares fit of a linear function to the sticking probability vs coverage curves in the coverage range beyond the break and then extrapolating the fit back to zero total coverage. The advantages of the latter method are its simplicity and the reduction of experimental noise by the averaging effect due to the fit. In addition, the determination of the ''desorption rates'' at zero total CO coverage means that a correction of the rate values with respect to the decreasing (1×5) surface fraction is not necessary. Moreover the results are not critically dependent on the precise shape of the hypothetical desorption-unaffected sticking probability vs coverage curve at 490 K. As can be seen from Figs. 7 and 8, the precondition of a temperature-independent initial sticking probability is satisfied for CO adsorption on both Ir{100}-(1×5) and (1×1). The island growth rate, r_g, at any total CO coverage is given by

$$r_g = z s_n, \tag{10}$$

where, z is the impingement rate; r_g can also be read at zero total coverage by means of the second method.

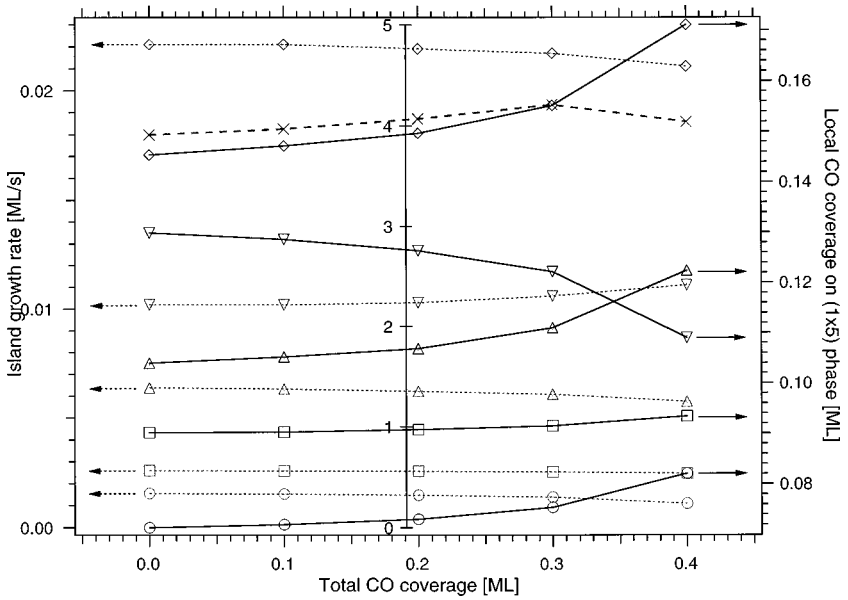

FIG. 12. Local CO coverage on the (1×5) phase, and the (1×1)-CO island growth rate relative to the estimated area of remaining (1×5) phase, shown as a function of the total CO coverage on an initially clean Ir{100}-(1×5) surface at 490 K. The central axis corresponds to the thick dashed curve, representing the variation in the reaction order, *n*.

Under the assumption of a coverage-independent desorption energy and first order desorption kinetics for CO, the local coverage on the (1×5) substrate can be derived simply by dividing the values for the desorption rates with the desorption rate constant k_d. The value for the desorption energy was chosen in order to obtain the optimum agreement between the coverages at the break positions and the local (1×5)-coverages obtained by dividing the experimental desorption rates by the corresponding rate constant. On the basis of $E_d=116$ kJ/mol one obtains $k_d=24\ s^{-1}$. The first order desorption pre-exponential of $6\times10^{13}\ s^{-1}$ for the (1×5) surface derives from the analysis of the isothermal desorption rates from that surface (cf. Fig. 4). Using these values it is possible to reproduce the coverage range of the break positions, as shown in Table I. The value used for E_d is much lower than the data for the (1×5)-surface in Fig. 3 and can be regarded as the lowest possible limit.

In addition the extrapolation method[27] was applied to the data of Fig. 9. The main advantage is that the local CO coverage and the island growth rate can be read at a series of different total CO coverages, yielding a set of values for the reaction order, *n*. Of course the sticking probability values have to be adjusted with respect to the remaining (1×5) surface fraction at any given total CO coverage, as shown in Fig. 12. The assumption for the adjustment, experimentally confirmed (Sec. III C), was that the growing (1×1) islands are covered with a constant local coverage of 0.5 ML. It is clear that the uncertainty in the determination of both the growth rate and the local CO (1×5) coverage increases the less (1×5) area there is remaining. Thus the data points in Fig. 12 are almost constant up to total coverages of about 0.2 ML. At higher coverages there is more noise and a reliable determination of the reaction order is no longer possible. Moreover it seems that the curves for the local CO coverages in Fig. 12 show a trend to higher values with increasing total CO coverage, i.e., with increasing (1×1) surface fraction. This could be a hint that the sticking probability curves in Fig. 9 are influenced by a small desorption rate from the growing (1×1) surface fraction. This cannot be proven nor quantified because of the inherent noise in the data, but the contribution is minor. From the curves in Fig. 12, a mean value for the reaction order of 4.2 was determined from 5 different total coverages.

2. Coverage dependent desorption energy

The coverage-dependent case starts with the assumption that the zero-coverage desorption energy from the (1×5) is around 150 kJ/mol, which is certainly the upper limit on the basis of the data presented in Fig. 3. Again the same first order pre-exponential of $6\times10^{13}\ s^{-1}$ is used. On this basis Langmuir isobars which include a linear dependence of the desorption energy were fitted to the experimental adsorption isobars from the (1×5) substrate. In this case only the interaction parameter was varied in order to obtain a least squares fit which best represented the experimental data. The calculated and experimental isotherms are shown in Fig. 5. In view of the simplicity of the model a reasonable fit was obtained, yielding a very high value of 109 kJ mol^{-1} ML^{-1} for the interaction energy. It has to be emphasized that this also represents the upper limit for this parameter and results from the discussion of two limiting cases. The local coverages on the (1×5) surface during the surface phase transition are estimated by calculating the equilibrium concentrations at 490 K and the fluxes used in the sticking probability experiments of Fig. 9. The extrapolated isobars for the 5 different fluxes used in the sticking probability experiments are shown in Fig. 13. The interpolated values, shown in Table I, are again within the coverage range of the break positions in Fig. 9.

Using the data in Table I the reaction order for the island growth could be determined for both limiting cases. Figure 14 shows a log–log plot of both sets of data. A strongly nonlinear dependence of the (1×1) island growth rate from the local CO coverage on the (1×5)-substrate is obtained for both cases. The reaction order is 3.9 for case 1 (constant

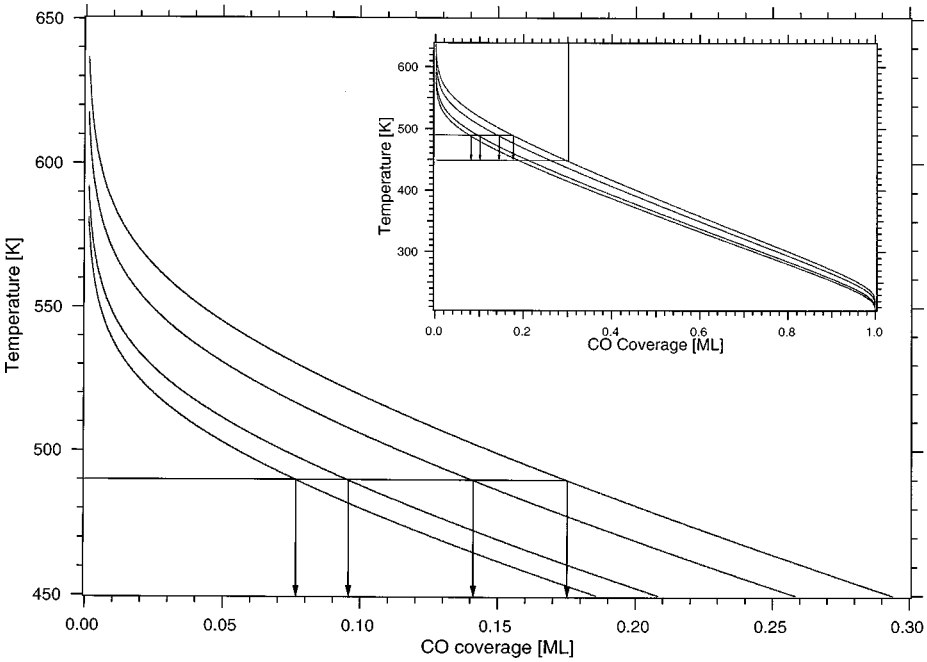

FIG. 13. Calculated Langmuir isobars for the beam fluxes used in the sticking probability experiments of Fig. 8. The same values for the parameters as used for the fit in Fig. 5 were employed. The arrows mark the interpolated local concentrations of CO on the (1×5) at 490 K.

desorption energy) and 5.8 for case 2. The linear coverage variation of the desorption energy with coverage represents an *additional* nonlinear term in the description of the equilibrium coverages, because it changes the exponent of the Arrhenius-expression for the desorption rate constant. We conclude, since we have analysed the data with two *limiting* assumptions, that the reaction order in the (1×1) growth expression is in the range $3.9\leqslant n\leqslant5.8$

C. Thermal energy atom scattering

Thermal energy atom scattering experiments were performed to investigate how CO is distributed laterally on the (1×5) surface during adsorption and surface restructuring. Figure 10 shows the relative specular helium reflectivity for CO adsorption onto an initially clean Ir{100}-(1×5) surface at 340 and 490 K, as a function of the total CO coverage. The corresponding sticking probability vs coverage curves are shown as the dashed trace (340 K) and the curve labeled b (490 K) in Fig. 8.

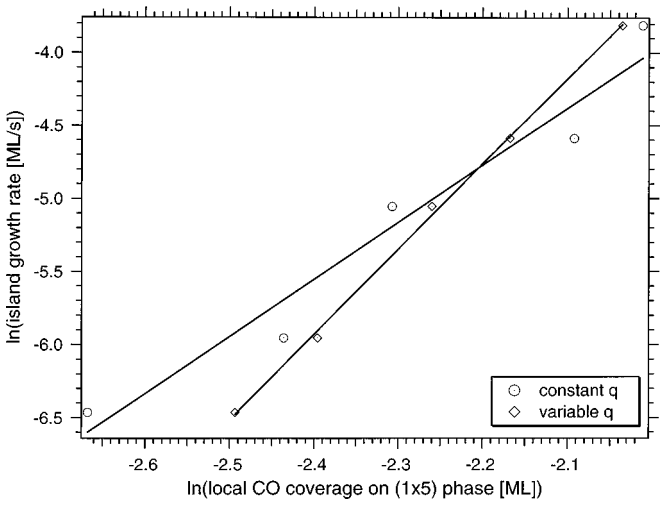

FIG. 14. Log–log plots of the (1×1) CO island growth rate as a function of local CO coverage on the (1×5) phase at $T_s=490$ K. The fit in the case of a coverage-independent desorption energy yields a reaction order of 3.9. Using a linearly coverage dependent E_d results in a value of $n=5.8$.

A sharp change in the scattering properties of the surface is indicative of a sudden structural change of the substrate rather than a change in the mean CO surface coverage. At $T_s=490$ K, the position where the adsorbate induced restructuring starts (around $\theta=0.1$ ML) is clearly indicated by a change in the slope of the He reflectivity (Fig. 10). Beyond this coverage, the reflectivity decreases linearly before tailing off as a total CO coverage of 0.5 ML is reached. The linear decrease in the specular He reflectivity with increasing θ_{CO} means that the local coverage within the growing islands is constant. Extrapolation of this linear region cuts the coverage axis at 0.5 ML, implying that this is the local coverage in the growing (1×1)-CO islands at 490 K. Thus, during the CO-induced restructuring processes, impinging CO molecules diffuse rapidly around the (1×5) surface and are either desorbed or cooperatively trapped into the growing (1×1) islands. These islands grow in size, with a constant *local* CO coverage of 0.5 ML, until the restructuring process is completed at a *total* CO coverage of 0.5 ML, at which point the entire surface is in the (1×1) phase.

In contrast, the TEAS curve during adsorption at 340 K exhibits a shape characteristic of random adsorption of CO molecules. A large cross section for He diffuse scattering from isolated adsorbed species results in the degree of overlap being strongly dependent on the adsorbate distribution. This is reflected in the coverage dependence of the specular He peak height ratio (or reflectivity), I/I_0, where I_0 is the specular peak height reflected from the clean surface. The diffuse cross section, Σ—the area ascribed to each adsorbate species which acts as a diffusely scattering patch—for an isolated CO molecule can be determined from

$$I/I_0=(1-\theta)^{n_s\Sigma}, \tag{11}$$

which relates the attenuation of the relative specular intensity to the average cross section for scattering He diffusely off the adsorbates.[28] θ is the CO coverage, n_s is the number of substrate atoms per unit area ($n_s = 1.32 \times 10^{15}$ atoms/cm^2 for Ir{100}), and so θn_s is the number of CO molecules per unit area on the (1×1) surface.

The experimental TEAS intensities for CO adsorption on the initially clean (1×5) substrate at 340 and 490 K are shown as the dashed curves in Fig. 10. At low coverages (below 0.04 ML) adsorption takes place mostly at defect sites. Since an Ir atom defect *and* a CO molecule at a defect would both scatter diffusely, there should be little or no change in the He specular scattering intensity at $\theta \leqslant 0.04$ ML, as actually observed. The solid curve in Fig. 10 represents the calculated TEAS intensity for random CO adsorption at 340 K on the initially clean (1×5) surface according to Eq. (11). A very good fit to the actual data is obtained, which indicates lattice-gas like adsorption, i.e., that the adsorbate is randomly distributed on the surface; there is no island formation. The best fit reveals a scattering cross section of 46 Å^2. This is somewhat smaller than the value of 71 Å^2 obtained for CO on Pt{100}-hex-*R* at 350 K.[29]

TEAS experiments have therefore revealed that the breaks observed in the sticking probability vs coverage curves (Fig. 8) are coincident with the onset of the CO induced lifting of the (1×5) reconstruction. The restructuring begins at a total coverage of $\theta \approx 0.1$ ML. At this point islands of (1×1)-CO begin to grow with a constant local CO coverage of 0.5 ML, until the entire surface is in the (1×1) phase. In contrast, at lower temperatures, outside the flux dependent sticking probability regime, and on the metastable (1×1) phase, lattice-gas like adsorption takes place—adsorbed CO does not tend to aggregate into islands.

IV. CONCLUSIONS

Sticking probability measurements as a function of the surface temperature and beam flux have been used to study the kinetics of CO chemisorption on both the (1×5) and the (1×1) surfaces of Ir{100}, as well as during the prevailing phase transformation. The initial sticking probability for CO on the Ir{100}-(1×5) surface is 0.55 and on the clean metastable (1×1) surface it is slightly higher, at 0.65. On both surfaces the sticking probability is constant up to a coverage of 0.1 ML, pointing to precursor-mediated adsorption on both substrates at ambient temperatures.

The rate of the CO induced $(1\times5)\rightarrow(1\times1)$ phase transformation for Ir{100} at surface temperatures between 480 and 510 K is described by a power law in the local CO coverage on the (1×5) phase. The apparent reaction order for this process, determined at 490 K, is 4.8 ± 0.9. The similarity between these results and those obtained for CO adsorption on Pt{100} indicate that the same basic underlying mechanism operates in the two systems. The only major difference is the much higher local CO coverage in the case of the Ir substrate during the phase transformation. This higher CO coverage is not surprising considering the comparatively large barrier to self-diffusion of Ir atoms on the {100} surface.[10]

Above a total coverage of 0.002 ML, the isosteric heat of adsorption on the (1×1) surface is found to be coverage independent, with a value of 196 ± 5 kJ/mol, except at coverages $\leqslant 0.002$ ML where it is higher due to adsorption on defect sites. In contrast, the isosteric heat of adsorption of CO on the (1×5) surface *without lifting the reconstruction* shows a pronounced coverage dependence in the range 0.002–0.006 ML. On Pt{100}-hex, the isosteric heat of adsorption was found to be 105 kJ/mol, independent of coverage. The lowest measured value for the heat of adsorption on the (1×5) surface of around 150 kJ/mol is the most realistic value for the zero coverage desorption energy from a defect-free surface.

The adsorption of CO on the metastable (1×1) substrate is thus energetically more favourable than on the reconstructed (1×5) surface. According to the measured heats of adsorption, 17 kJ/mol (with respect to Ir surface atoms) is gained upon trapping chemisorbed CO from the (1×5) and converting it into the (1×1) phase. This difference in energy, which is the driving force for the CO-induced lifting of the reconstruction, is smaller than was determined for Pt{100}-hex and (1×1).[11]

Much higher local CO coverages were observed on Ir{100}-(1×5) during (1×1) island growth (0.05–0.13 ML) than on Pt{100} [0.01–0.03 ML (Refs. 11, 12)], as reflected by both the sticking probability vs CO-coverage curves and the simultaneously recorded TEAS intensity curves. TEAS data show that the local coverage within the growing (1×1) islands during the CO induced $(1\times5)\rightarrow(1\times1)$ phase transformation is constant at 0.5 ML.

As a result of the large differences in catalytic activity of different surface phases of a metal surface, the surface restructuring induced by adsorbates during a catalytic reaction can lead to kinetic oscillations.[30] The nonlinear term in the growth law, $r_{1\times1} = c(\theta_{\mathrm{hex}})^n$, is a crucial factor in the appearance of oscillations in a series of reactions on Pt{100}: NO+CO;[14,15] CO+O$_2$;[16,17] and NO+H$_2$.[18,19] These reactions generally exhibit oscillatory behavior only at pressures and temperatures where the lifetime of at least one of the reactants is much shorter on one of the phases than on the other, and where the (1×1) to hex transformation rate is rapid. Although there is currently no literature concerning oscillatory reactions on Ir{100}, the findings of the current study strongly suggest that oscillatory behavior would be observed, but only at temperatures above ~900 K, where the (1×1) to (1×5) transformation is fast, and at high reactant partial pressures, to maintain coverages sufficiently high to drive the phase transformation. With the aid of the experimental isobars on the Ir{100}-(1×5) surface (Fig. 5) it is possible to estimate the flux of CO required to maintain a sufficiently high coverage to drive the phase transition at elevated temperatures. For a sample temperature of 1000 K a CO partial pressure of around 30 mbar is required in order to achieve a total CO coverage of 0.2 ML—sufficient to lift the reconstruction. We would anticipate the observation of oscillations in CO oxidation on Ir{100} under these conditions.

ACKNOWLEDGMENTS

We acknowledge the Oppenheimer Trust for a research studentship (TA), the FWF, Vienna, for an Erwin Schrödinger Scholarship (BK), Shell Research and Technology Centre, Amsterdam for a studentship (AVW), and the EPSRC for an equipment grant. We are grateful to Christian Resch and Victor Ostanin for helpful discussions and for technical support.

[1] A. Ignatiev, A. V. Jones, and T. N. Rhodin, Surf. Sci. **30**, 573 (1972).
[2] K. Heinz, G. Schmidt, L. Hammer, and K. Müller, Phys. Rev. B **32**, 6214 (1985).
[3] N. Bickel and K. Heinz, Surf. Sci. **163**, 435 (1985).
[4] J. Küppers and H. Michel, Appl. Surf. Sci. **3**, 179 (1979).
[5] M. A. van Hove, R. J. Koestner, P. C. Stair, J. P. Biberian, L. L. Kesmodel, I. Bartos, and G. A. Somorjai, Surf. Sci. **103**, 189 (1981).
[6] T. N. Rhodin and G. Broden, Surf. Sci. **60**, 466 (1976).
[7] G. Kisters, J. G. Chen, S. Lehwald, and H. Ibach, Surf. Sci. **245**, 65 (1991).
[8] J. T. Grant, Surf. Sci. **18**, 228 (1969).
[9] P. Gardner, R. Martin, R. Nalezinski, C. L. A. Lamont, M. J. Weaver, and A. M. Bradshaw, J. Chem. Soc., Faraday Trans. **91**, 3575 (1995).
[10] G. Boisvert, L. J. Lewis, M. J. Puska, and R. M. Nieminen, Phys. Rev. B **52**, 9078 (1995).
[11] A. Hopkinson, J. M. Bradley, X. C. Guo, and D. A. King, Phys. Rev. Lett. **71**, 1597 (1993).
[12] A. Hopkinson, X. C. Guo, J. M. Bradley, and D. A. King, J. Chem. Phys. **99**, 8262 (1993).
[13] A. T. Pasteur, St. J. Dixon-Warren, and D. A. King, J. Chem. Phys. **103**, 2251 (1995).
[14] A. Hopkinson and D. A. King, Chem. Phys. **177**, 433 (1993).
[15] A. Hopkinson and D. A. King, Faraday Discuss. **6**, 255 (1993).
[16] M. Gruyters, T. Ali, and D. A. King, Chem. Phys. Lett. **232**, 1 (1995).
[17] M. Gruyters, T. Ali, and D. A. King, J. Phys. Chem. **100**, 14417 (1996).
[18] M. Gruyters, A. T. Pasteur, and D. A. King, J. Chem. Soc., Faraday Trans. **92**, 2941 (1996).
[19] A. V. Walker, M. Gruyters, and D. A. King, Surf. Sci. **384**, L791 (1997).
[20] M. Gruyters and D. A. King, J. Chem. Soc., Faraday Trans. **93**, 2947 (1997).
[21] X. C. Guo, J. M. Bradley, A. Hopkinson, and D. A. King, Surf. Sci. **310**, 163 (1994).
[22] D. A. King and M. G. Wells, Surf. Sci. **29**, 245 (1972).
[23] J. K. Fremerey, J. Vac. Sci. Technol. A **3**, 1715 (1985).
[24] Q. Ge, N. Marzouri, M. C. Payne, and D. A. King, Surf. Sci. (in press).
[25] Y. Y. Yeo, C. E. Wartnaby, and D. A. King, Science **268**, 1731 (1995).
[26] W. A. Brown, R. Kose, and D. A. King, Chem. Rev. **98**, 797 (1998).
[27] X. C. Guo and D. A. King, Surf. Sci. **302**, L251 (1994).
[28] C. Poelsema and G. Comsa, *Scattering of Thermal Energy Atoms* (Springer, Berlin, 1989).
[29] A. T. Pasteur, X. C. Guo, T. Ali, M. Gruyters, and D. A. King, J. Chem. Phys. **366**, 564 (1996).
[30] G. Ertl, Science **254**, 1750 (1991).